The Astrophysical Journal, 677:676–682, 2008 April 10

ASYMMETRIC SOLAR WIND ELECTRON SUPERTHERMAL DISTRIBUTIONS

R. Gaelzer
Instituto de Física e Matemática, Caixa Postal 354-Campus UFPel, 96010-900 Pelotas-RS, Brazil; rudi@ufpel.edu.br

L. F. Ziebell
Instituto de Física, UFRGS, Caixa Postal 15051, 91501-970 Porto Alegre-RS, Brazil

A. F. Viñas
NASA Goddard Space Flight Center, Greenbelt, MD 20771

P. H. Yoon[1]
Institute for Physical Science and Technology, University of Maryland, College Park, MD 20742

AND

C.-M. Ryu
Department of Physics, Pohang University of Science and Technology, Pohang, South Korea
Received 2007 September 4; accepted 2007 November 22

ABSTRACT

Electron distributions with various degrees of asymmetry associated with the energetic tail population are commonly detected in the solar wind near 1 AU. By numerically solving one-dimensional electrostatic weak turbulence equations the present paper demonstrates that a wide variety of asymmetric energetic tail distributions may result. It is found that a wide variety of asymmetric tail formation becomes possible if one posits that the solar wind electrons are initially composed of thermal core plus field-aligned counterstreaming beams, instead of the customary thermal population plus a single beam. It is shown that the resulting nonlinear wave-wave and wave-particle interactions lead to asymmetric nonthermal tails. It is found that the delicate difference in the average beam speeds associated with the forward versus backward components is responsible for the generation of asymmetry in the energetic tail.

Subject headings: interplanetary medium — solar wind

1. INTRODUCTION

The electron velocity distributions detected in the solar wind near 1 AU and in the upstream region of the Earth's bow shock are typically observed to be made of low-energy and dense thermal core plus two tenuous but hot superthermal populations, the *halo*, which is present at all pitch angles, and the *strahl*, which is a highly anisotropic, field-aligned population (Montgomery et al. 1968; Feldman et al. 1975; Lin et al. 1981, 1986; Pilipp et al. 1987a, 1987b; Fitzenreiter et al. 1990, 1998; Ergun et al. 1998; Ogilvie et al. 1999; Pierrard et al. 2001a; Pagel et al. 2005). In the literature, such particle distributions with thermal core plus the energetic tail are often modeled by the so-called κ-distribution (Vasyliunas 1968; Summers & Thorne 1991; Mace & Hellberg 1995; Yin et al. 1998). However, the actual electron distributions measured in the solar wind (and to some degree, in the upstream region of the bow shock) often feature highly asymmetric forms such that they cannot be simply fit by κ-models.

The physical origin of the strahl or the isotropic halo electron populations that can be clearly distinguished from the Maxwellian core distribution remains as somewhat of a mystery to this day. In the literature most theories that attempt to address the origin of superthermal electrons usually start from the consideration of the altitude-dependent collisional dynamics (Scudder & Olbert 1979a, 1979b; Canullo et al. 1996; Lie-Svendsen et al. 1997; Pierrard et al. 1999, 2001a, 2001b; Landi & Pantellini 2001; Dorelli & Scudder 2003; Vocks & Mann 2003; Vocks et al. 2005; Maksimovic et al. 2005).

The formation of the distinguishing features of the VDFs (velocity distribution functions) is usually described by the exospheric theory of the solar wind electrons (Pilipp et al. 1987a; Pierrad et al. 2001a). According to this theory, the core population is composed of low-temperature electrons trapped within the ambipolar thermoelectric potential well of the heliosphere, whereas the halo and strahl populations are composed of high-energy electrons that escape the potential barrier. The strong anisotropy of the strahl is understood as the result of pitch-angle focusing along the magnetic field line, in the antisunward direction, due to the conservation of the magnetic moment. On the other hand, the isotropy of the halo is not well understood, and it has been long established that the strahl distribution is broader than is expected from conservation of the adiabatic invariant alone, an effect that cannot be fully explained by Coulomb collisions, since that electron population at the spacecraft site is largely collisionless (Pilipp et al. 1987b; Pagel et al. 2007).

In an attempt to explain the formation of both the halo and strahl populations, as well as the observed pitch-angle diffusion of the strahl electrons, Vocks & Mann (2003) and Vocks et al. (2005) studied the quasilinear diffusion of a κ-distribution function in the presence of whistler waves propagating both in the sunward and antisunward directions. Although they were able to obtain distributions that resemble the observed ones, their model was not fully self-consistent. In particular, they did not consider the effect of wave-particle interactions on the whistler waves, which should limit the total energy of the resonant wave available for pitch-angle scattering due to the finite value of the damping rate (Saito & Gary 2007). Moreover, since the observed distributions are measured with time intervals that can range from several seconds up to minutes, depending on the pitch-angle

[1] Department of Physics, Pohang University of Science and Technology, Pohang, South Korea.

resolution, higher order nonlinear effects, such as wave-wave and nonlinear wave-particle interactions, should be included for a complete kinetic description.

In contrast to these theories, in the present paper, we look for collective mechanism(s) that include nonlinear effects as a potential explanation for the generation of superthermal population. As the solar wind expands into the surrounding interplanetary medium, the faster electrons outpacing the slow ones will inevitably lead to the formation of field-aligned beams. The beam electrons will excite plasma instability, which in turn will slow down the beams. In short, there will be a constant "struggle" between the quasilinear relaxation and the time-of-flight beam reformation process. Thus, we expect that, while collisional dynamics may be important very close to the solar surface, in most of the interplanetary space, the collective dynamical processes may play an important role in the electron scattering processes. We thus investigate the role of plasma instability and turbulent dynamical processes in the formation of the superthermal tail population.

A fundamental assumption in our theory is the presence of an initial-time population inversion [i.e., $\partial f_e(v, 0)/\partial v_\parallel > 0$, where f_e is the electron VDF] due to the beam. While the observational data do not show such a feature, we want to point out the fact that the ensuing quasilinear diffusion process, followed by the nonlinear effects of three-wave decay and nonlinear wave-particle scattering, responsible for the high-energy tail formation in our theory, takes a total amount of time that is smaller, by a factor around 10, than the usual sampling rate of present-day spacecraft, which can be of the order of several seconds. Consequently, any population inversion will be completely diffused by the time the spacecraft obtains a full VDF, and the observed distribution will have a substantial amount of nonlinearly scattered particles.

The basic demonstration that turbulent processes lead to these hot plasma populations has already been accomplished in the papers by Yoon et al. (2006) and Rhee et al. (2006). The focus of the present discussion is on the question of what leads to the observed asymmetry associated with the solar wind superthermal electrons. In the present paper we thus put forth a theory in which the highly asymmetric energetic tail distribution may be the result of dense thermal core electrons interacting with not just one field-aligned energetic electron beam component, but rather a pair of initially counterstreaming energetic but tenuous electron beam populations. The resulting nonlinear interactions among the electrons with the Langmuir and ion-sound turbulence leads to the observed highly asymmetric superthermal tail population.

To demonstrate this we have carried out a series of numerical analyses in which self-consistent weak turbulence equations are solved for initial electron distribution consisting of three components—the background plus the forward and backward traveling electron beam populations. It is shown that the resulting development of Langmuir turbulence excited by the interaction among the counterstreaming electrons and the background thermal distribution of electrons leads to the asymmetric energetic tail distribution. From this we suggest that the observed asymmetric superthermal electrons in the solar wind may be the result of turbulence acceleration by self-consistently generated Langmuir waves excited by the three-component electron distribution system associated with the solar wind.

The plan of the paper is as follows. In § 2 some observational results from the *WIND* spacecraft are presented and discussed. In the context of these observations § 3 presents the basic theory of weak plasma turbulence and the model adopted in this work, followed by the main results obtained from the model. Finally, § 4 discusses the results and shows our conclusions.

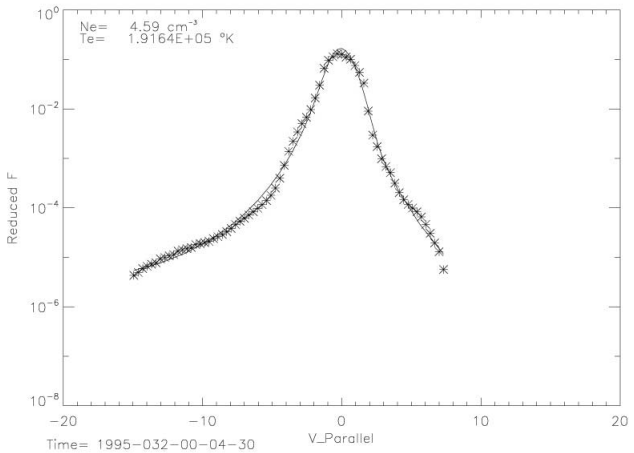

FIG. 1.—Sample of electron distribution detected in the solar wind featuring a highly asymmetric tail population. The distribution is given in arbitrary units and, $v_\parallel$ is normalized to $\mathcal{V}_{\rm scale} = 2 \times 10^8$ cm s^{-1}, which is a thermal speed corresponding to a temperature of about 1.3×10^5 K, typical of solar wind temperatures.

2. *WIND* SWE-VEIS ELECTRON OBSERVATIONS

The electron three-dimensional (3D) VDF measurements used in our study have been obtained from the 3 s time resolution data of the *WIND* SWE VEIS spectrometer (details of the instrument characteristics can be found in Ogilvie et al. 1995). The VEIS spectrometer consists of six programmable analyzers that form an array of three pairs of mutually orthogonal sensors that measures electrons in the energy range from 7 eV to 25 keV in 16 energy steps with an energy resolution of about 6%. However, for solar wind electron studies the effective energy range has been set from 10 eV to 3 keV. Each sensor full energy sweep takes 0.5 s, which implies that the highest time resolution moment is determined in 0.5 s, but for statistical purposes, the moments have been averaged out to the full satellite spin period of 3 s. The moment calculations have been corrected by the spacecraft potential (which usually ranges between 3 and 15 V, depending on solar conditions) using either the proton and α measurements from the *WIND* SWE MIT Faraday cup or the electron density estimates of the plasma frequency line from the *WIND* WAVES experiment.

The VDFs presented in this paper have been shifted into the solar wind frame using the proton bulk velocity interpolated to the electron times, and the higher order moments (e.g., $\boldsymbol{P}_e$ and $\boldsymbol{Q}_e$) estimated have been calculated in that frame. The VDF data sets used in this study are the reduced $F(v_\parallel)$ distribution functions obtained by folding the original 3D distributions into the $(v_\parallel, v_\perp)$ space (e.g., assuming the gyrotropy condition) using the measured 3 s magnetic field averages and then integrating the two-dimensional (2D) distributions in the $v_\perp$ space.

Figures 1 and 2 show two samples of typical reduced electron velocity distribution functions during a long-orbit excursion of the *WIND* spacecraft to L1 in the solar wind, which occurred on 1995 February 1. The plots also display fits (*solid line*) to the observed distributions (*asterisk*) using a model of a superposition of a Mawellian (core) and a κ-distribution (halo) models. Each model distribution function features a drift relative to the reference frame (δU_c for the core and δU_h for the halo), in such a way that the condition of zero net current ($n_c\,\delta U_c + n_h\,\delta U_h = 0$) is satisfied. The best fitting was obtained by the minimization of the χ^2 function, and it provides the best values of all the relevant physical parameters, including the drift speeds and the κ-parameter. The data analysis and fitting procedure are extensively detailed in Nieves-Chinchilla & Viñas (2008).

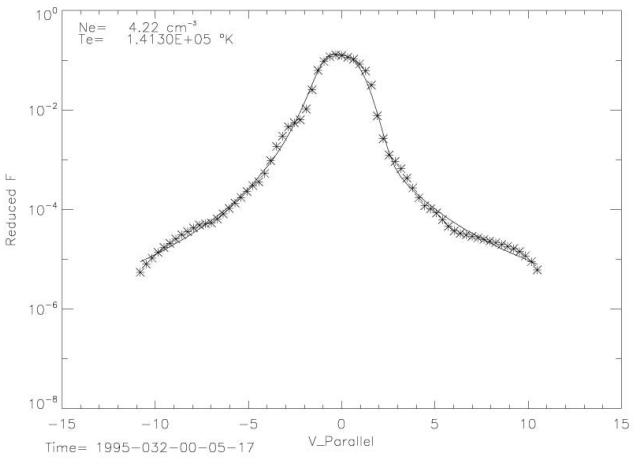

FIG. 2.—Sample electron distribution detected in the solar wind featuring quasi-symmetric tail population. The distribution and $v_\parallel$ have the same normalization as in Fig. 1.

The electron VDF shown in Figure 1 clearly shows asymmetric pronounced tails along the magnetic field, which is an indication of the heat flux. The parallel velocity ($v_\parallel$) is obtained by decomposing the full velocity vector $\boldsymbol{v}$ relative to the local magnetic field $\boldsymbol{B}$, so that $\boldsymbol{v}_\parallel = \boldsymbol{v}\cdot\boldsymbol{B}/|\boldsymbol{B}|$ in the GSE coordinate system, whose x-component points from Earth to the Sun. In contrast, the electron VDF displayed in Figure 2 features a quasi-symmetric superthermal tail population. For the two VDFs selected on Figures 1 and 2, the $\boldsymbol{B}$-field components are $\boldsymbol{B} = (4.560, -2.355, 2.352)$ nT and $\boldsymbol{B} = (4.812, -2.910, -1.014)$ nT, respectively. Note that the fields are mostly in the x-direction, which in GSE is pointing toward the Sun, but the heat flux is mainly from the Sun to the Earth. Therefore, we expect the distributions to be skewed in the negative-$v_\parallel$ direction as shown on Figures 1 and 2.

3. THEORY AND RESULTS

The basic theoretical framework is the self-consistent weak turbulence equations that describe nonlinear interactions among Langmuir and ion-sound mode, as well as with the particles. In the present analysis, we resort to one-dimensional approximation and assume that only electrostatic interaction is of importance. The equations of weak turbulence theory can be found in the papers by Yoon et al. (2006) and Rhee et al. (2006). These consist of Langmuir and ion-sound wave kinetic equations and the particle (electron) kinetic equation. Since the basic equations to be numerically solved are the same as in the paper by Yoon et al. (2006), we do not repeat them here. We simply note that the normalization of the physical quantities in the present paper is such that dimensionless time, speed, and the wavenumber are given by

$$\begin{aligned} T &= \omega_{pe} t, \\ \mathcal{V} &\rightarrow v/v_{Te}, \\ \mathcal{K} &\rightarrow k v_{Te}/\omega_{pe}. \end{aligned} \tag{1}$$

That is, by simply referring to $\mathcal{V}$ and $\mathcal{K}$, we mean, respectively, the normalized quantities as defined above. In equation (1), $\omega_{pe} = (4\pi \hat{\boldsymbol{n}} e^2/m_e)^{1/2}$ is the plasma frequency, $\hat{\boldsymbol{n}}$, e, and m_e being the ambient density, unit electric charge, and electron mass, respectively; v is a one-dimensional velocity; $v_{Te} = (2T_e/m_e)^{1/2}$ is the electron thermal speed, T_e being the electron temperature in units of energy; and k is the one-dimensional wavenumber.

The basic physics of a self-consistent theory of superthermal tail generation during the beam-plasma interaction has been elucidated in the papers by Yoon et al. (2005, 2006) and Rhee et al. (2006). In these papers, the interaction of an initially Gaussian distribution of energetic electron beam with thermal electrons is considered. It was shown that the final asymptotic electron distribution resembled the well-known κ-distribution (Vasyliunas 1968; Summers & Thorne 1991; Mace & Hellberg 1995; Yin et al. 1998) with a non-Gaussian energetic tail. The physical mechanism responsible for the acceleration of electrons was also identified as the so-called spontaneous scattering of electrons off thermal ions, mediated by Langmuir turbulence of intermediate wavelengths. The spontaneous scattering process is a nonlinear wave-particle interaction that is operative only when the discrete-particle nature of the plasma is taken into account.

In spite of the fact that the basic underlying physics of superthermal electron formation is understood, the theory discussed in the papers by Yoon et al. (2005, 2006) and Rhee et al. (2006) is limited in that the asymptotic quasi-κ-distribution that emerges from such a theory is more or less invariant in terms of the degree of asymmetry associated with the forward-going (positive velocity) versus backward-propagating (negative velocity) particles. In order to explain a wide variety of asymmetric energetic tail distribution typically observed in the solar wind one must modify the fundamental assumptions.

In view of the fact that modeling the solar wind as a core Maxwellian plus a single beam does not give us enough freedom to generate a wide variety of asymmetric tail distribution, we have decided to allow for the presence of a small but oppositely directed secondary beam component. We have thus revisited our previous model considered by Yoon et al. (2005, 2006) and Rhee et al. (2006) and replaced the initial electron distribution with a different initial configuration in which a secondary backward-propagating Gaussian beam is added to the original configuration of Gaussian beam plus the background.

The justification for the presence of counterstreaming electrons is more than academic. At 1 AU the interplanetary magnetic field structure may be rather complicated, and especially when both foot points of the field line loops are located on the Sun, then the field-aligned motion of the electrons may indeed be characterized as counterstreaming. Sufficiently close to the Earth electron foreshock, the reflected electrons off the cross-shock electrostatic potential may coexist with the incoming solar wind electrons. Sunward-propagating beams can also be observed inside closed magnetic field structures, which can be generated by flare-induced interplanetary shock waves (Pilipp et al. 1987b). The observation of counterstreaming superthermal electrons is also used as a signature of a large coronal mass ejection (Shodhan et al. 2000). In such situations, the assumption of a counterstreaming population is again justifiable.

As we shall demonstrate subsequently, the resulting numerical solutions with the initial counterstreaming electrons plus the dense core population are quite extraordinary in that a wide-ranging asymmetry associated with the energetic electron tail distribution can be obtained, which could not have been foreseen a priori. In what follows we showcase two extreme situations. One case corresponds to a highly asymmetric energetic tail distribution, while in the second case, we demonstrate symmetric tail distribution. However, we hasten to point out that we were also able to generate wide-ranging asymmetric distributions between the two extremes.

The input physical parameters are the ratio of the forward-propagating electron beam density to the background number density, n_f; ratio of the backward-propagating electron beam density

to the background number density, n_b; ratio of forward and backward beam speed to thermal speed, U_f and U_b; ion-to-electron temperature ratio, τ; ion-to-electron mass ratio, M; and the plasma parameter g:

$$\begin{aligned} n_f &= \hat{\boldsymbol{n}}_f/\hat{\boldsymbol{n}}_0, \\ n_b &= \hat{\boldsymbol{n}}_b/\hat{\boldsymbol{n}}_0, \\ U_f &= V_f/v_{Te}, \\ U_b &= V_b/v_{Te}, \\ \tau &= T_i/T_e, \\ M &= m_i/m_e, \\ g &= 1/\hat{\boldsymbol{n}}\lambda_{\mathrm{D}}^3. \end{aligned} \tag{2}$$

Here $\lambda_{\mathrm{D}}^2 = T_e/(4\pi\hat{\boldsymbol{n}}e^2)$ is the square of the electron Debye length. In the present analysis we assume that Gaussian thermal spreads associated with the core electrons, and the counterstreaming beams are the same. Of the above, we assume that $\tau = \frac{1}{7}$, $m = 1836$, and $g = 5\times10^{-3}$. We do not vary these quantities in the subsequent numerical analysis.

The initial electron distribution and stationary ion distribution are given, respectively, in normalized form, by

$$\begin{aligned} f_e(\mathcal{V},0) &= \pi^{-1/2}\left\{\exp\left(-\mathcal{V}^2\right) + n_f \exp\left[-\left(\mathcal{V}-U_f\right)^2\right]\right\} \\ &\quad + \left\{n_b \exp\left[-\left(\mathcal{V}-U_b\right)^2\right]\right\}, \\ f_i(\mathcal{V}) &= \sqrt{\frac{M}{\pi\tau}}\exp\left(-\frac{M\mathcal{V}^2}{\tau}\right). \end{aligned} \tag{3}$$

The turbulence intensity is normalized according to the convention

$$I_{\sigma\alpha}(\mathcal{K}) = \frac{gI_k^{\sigma\alpha}}{8\sqrt{2}m_e v_{Te}^2}, \tag{4}$$

where $I_k^{\pm\alpha}/8\pi = \left\langle \delta E_{\pm}^{\alpha 2}\right\rangle_k/8\pi$ is the ensemble average of the spectral wave electric field energy density corresponding to mode α propagating in the forward (+) or backward (−) direction with respect to the beam propagation direction. For electrostatic turbulence, $\alpha = S, L$, where S, L correspond to the ion-sound and Langmuir modes, respectively. The initial perturbation is specified according to the spontaneous emission formula and is given by

$$\begin{aligned} I_{\pm L}(\mathcal{K},0) &= \frac{g}{2^6\sqrt{2}\pi^2}\frac{1}{1+3\mathcal{K}^2/2}, \\ I_{\pm S}(\mathcal{K},0) &= \frac{g\mathcal{K}^2}{2^7\sqrt{2}\pi^2}\sqrt{\frac{1+\mathcal{K}^2/2}{1+3\mathcal{K}^2/2}} \\ &\quad \times \left.\frac{e^{-\mathcal{V}^2} + (M/\tau)^{1/2}e^{-M\mathcal{V}^2/\tau}}{e^{-\mathcal{V}^2} + \tau^{-1}(M/\tau)^{1/2}e^{-M\mathcal{V}^2/\tau}}\right|_{\mathcal{V}=\mathcal{V}_r}, \\ \mathcal{V}_r &= \sqrt{\frac{1+3\tau}{M\left(2+\mathcal{K}^2\right)}}. \end{aligned} \tag{5}$$

We have solved the weak turbulence equation with the standard leap-frog method with the time increment $\Delta T = 0.01$. We take 201 velocity grid points and 101 grid points for the wavenumbers. The wave intensities are computed over the positive $\mathcal{K}$ space, but we plot backward-propagating wave intensities, $I_{-L}(\mathcal{K})$ and $I_{-S}(\mathcal{K})$, over the negative $\mathcal{K}$ space by invoking the symmetry relations, $I_{\pm L}(\mathcal{K}) = I_{\mp L}(-\mathcal{K})$ and $I_{\pm S}(\mathcal{K}) = I_{\mp S}(-\mathcal{K})$.

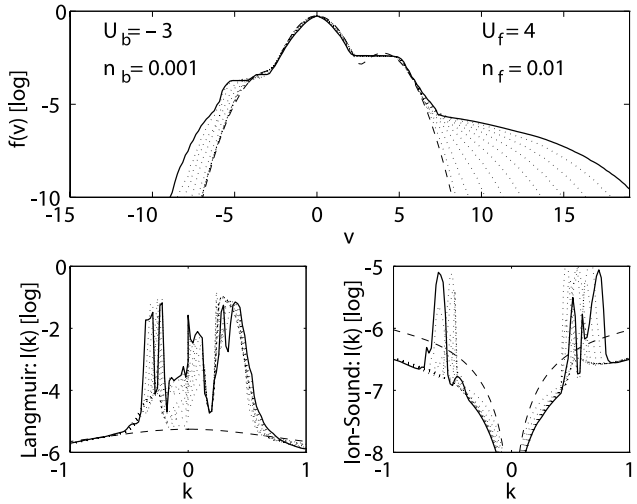

FIG. 3.—Time evolution of electron distribution vs. $\mathcal{V} = v/v_{Te}$ (*top*), and Langmuir (*bottom left*) and ion-sound (*bottom right*) mode spectral wave energy intensities vs. $\mathcal{K} = kv_{Te}/\omega_{pe}$. The final time step corresponds to normalized time $T = 1\times10^4$, with every $\Delta T = 1000$ intermediate time step plotted with dashes. Forward beam is characterized by $n_f = 0.01$ and $U_f = 4$, while the parameters for the backward beam are $n_b = 0.001$ and $U_b = -3$.

3.1. *Asymmetric Tail*

In the first example, we consider the following set of input parameters:

$$\begin{aligned} U_f &= 4, \\ U_b &= -3, \\ n_f &= 1\times10^{-2}, \\ n_b &= 1\times10^{-3}. \end{aligned} \tag{6}$$

Figure 3 shows the time evolution of the total electron distribution $f_e(\mathcal{V})$ versus v (*top*), and Langmuir (*bottom left*) and ion-sound (*bottom right*) mode spectral wave energy intensities, $I_L(\mathcal{K})$ and $I_S(k)$, versus k. The final time step corresponds to normalized time $T = 1\times10^4$, with every $\Delta T = 1000$ intermediate time step plotted with dashes. For the present choice of the backward beam speed $U_b = -3$, which is slightly less than the forward beam speed, $U_f = 4$, and for the forward beam density sufficiently higher than the backward beam density, $n_f = 0.01$ and $n_b = 0.001$, we find that the asymptotic state of the electron distribution function is highly asymmetric in that the positive v range features an extended higher energy tail, but the negative v space has virtually no energetic tail distribution.

To see whether the highly asymmetric tail formation is the result of the differences in the magnitude of beam speed or the density, we have varied U_b and n_b separately, but we found that it is the beam speed that determines the degree of asymmetry associated with the energetic tail. To show this, in Figure 4 we display the results with the same input parameters as in Figure 3 (see eq. [6]), except that

$$n_b = 0.005. \tag{7}$$

Note that the overall feature associated with the electron distribution function is qualitatively similar to Figure 2 in that positive $\mathcal{V}$ space has extended tail, while the negative $\mathcal{V}$ has no energetic non-Gaussian tail. As a matter of fact, the slight increase in the

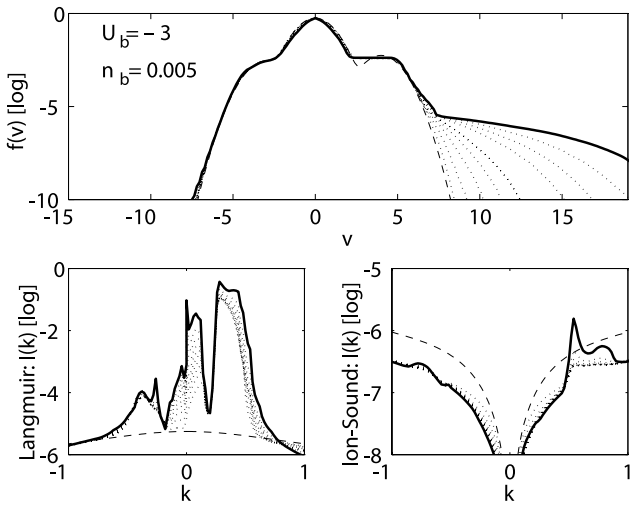

FIG. 4.—Same as Fig. 3, except that the backward beam density is raised to 0.5%.

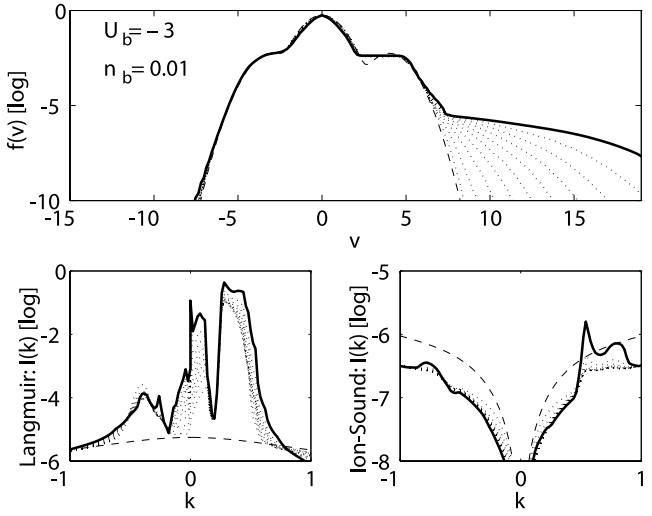

FIG. 5.—Same as Fig. 3, except that the backward beam density is further raised to 1%.

backward beam density has resulted in the suppression of what little non-Gaussian feature the electrons with negative $\mathcal{V}$ had before. The increase in n_b has concomitantly resulted in a noticeable increase in the population of energetic electrons with positive $\mathcal{V}$.

To further test the hypothesis that the change in the backward beam density does not qualitatively alter the asymmetry associated with the energetic tail distribution, we now consider the equal density counterstreaming beam situation, i.e.,

$$n_b = 0.01. \tag{8}$$

The numerical solutions are shown in Figure 5. As the reader may appreciate, the results are virtually the same as Figure 4. From this, we tentatively conclude that the asymmetry in the counterstreaming beam speeds is responsible for generating asymmetric energetic tails.

3.2. *Symmetric Tail*

To further confirm the above tentative finding, we now consider equal beam speed counterstreaming situation with the beam parameters,

$$\begin{aligned} U_f &= 4, \\ U_b &= -4, \\ n_f &= 1 \times 10^{-2}, \\ n_b &= 1 \times 10^{-3}. \end{aligned} \tag{9}$$

Figure 6 is in the same format as Figure 3. For the present choice of the beam speeds $U_b = -4$ and $U_f = 4$, and for $n_f = 0.01$ and $n_b = 0.001$, we find that the asymptotic state of the electron distribution function features a quasi-symmetric high-energy tail population.

We now increase the backward beam density to

$$n_b = 0.005. \tag{10}$$

The numerical result is displayed in Figure 7. As one can see, the degree of symmetry in the forward ($\mathcal{V} > 0$) and backward ($\mathcal{V} < 0$) propagating electron tail populations has somewhat increased when compared with Figure 6.

Finally we move on to the case of equal counterstreaming beam speeds and densities, namely,

$$n_b = 0.01. \tag{11}$$

The numerical solutions shown in Figure 8 correspond to a highly symmetric energetic tail distribution for the particles and symmetric wave spectra.

Although we have chosen only two representative cases, we have actually considered other cases as well. Depending on the backward beam speed U_b, we found that the degree of asymmetry associated with the energetic tail greatly varies. However, the dependence of the asymmetry on U_b is not a simple linear relationship. For instance, as the previous Figures 3–8 show, the case of $U_b = -4$ led to a symmetric two-sided tail distribution, whereas the case of $U_b = -3$ produced an almost one-sided tail. From this, one may naively expect that a further reduction of U_b from $U_b = -3$ to, say, $U_b = -2.5$, may lead to even more prominent one-sided tail in the positive $\mathcal{V}$-direction. However, this is not the case at all. In fact, we found that the reduction of $U_b = -3$ to something like $U_b = -2.5$ actually caused the negative $\mathcal{V}$ tail to grow back. The case of $U_b = -3$ actually corresponds to the extremum case where the energetic tail is almost

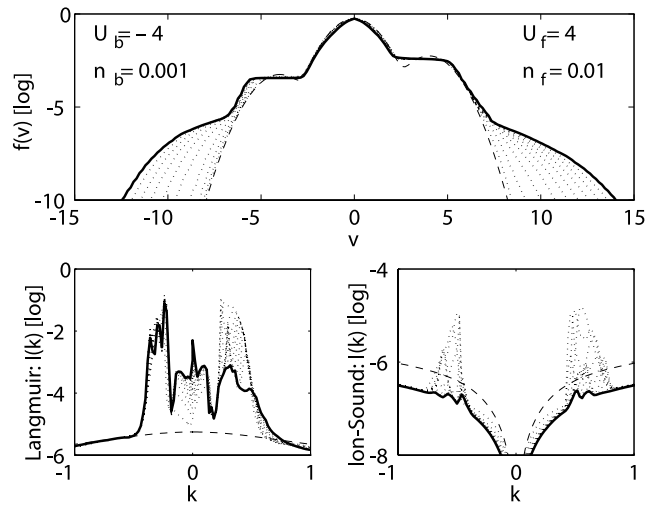

FIG. 6.—The initial forward beam parameters are $n_f = 0.01$ and $U_f = 4$, while the parameters for the backward beam are $n_b = 0.001$ and $U_b = -4$.

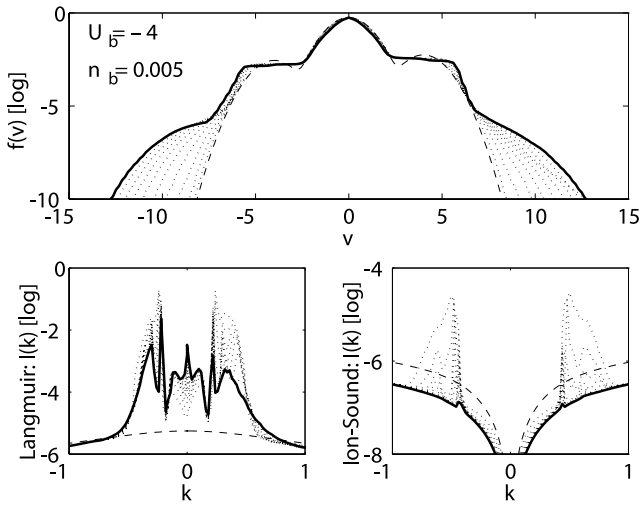

FIG. 7.—Same as Fig. 6, except that the backward beam density is raised to 0.5%.

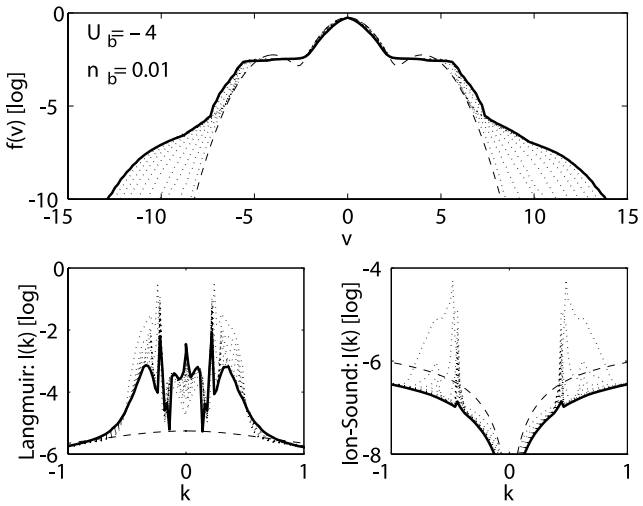

FIG. 8.—Same as Fig. 6, except that the backward beam density is further raised to 1%. This situation corresponds to equal counterstreaming beam speeds and densities.

completely one-sided. This finding suggests that the energization of the electrons and the formation of an asymmetric tail population is not a simple phenomenon to be explained intuitively.

An important order of magnitude analysis that can be made concerns the typical amount of time required for a substantial high-energy tail to form. All our results were displayed with a final normalized time of $T = 10^4$. Assuming an electron density of $n_e \simeq 5$ cm^{-3}, usually observed by the *WIND* spacecraft (see Figs. 1 and 2), we have a typical plasma frequency of 20 kHz in the solar wind at 1 AU. This means that the final distribution functions that we obtained correspond to a total real time around 0.08 s smaller by a factor of at least 10 than the spin period of 3 s of the *WIND* spacecraft (see discussion in § 2). Therefore, it is reasonable to assume that the observed VDFs contain a large amount of nonlinearly scattered particles, as one would expect from our theory.

4. CONCLUSIONS AND DISCUSSION

The electron velocity distribution functions detected in the solar wind near 1 AU and in the upstream region of the Earth's bow shock are typically observed to be made of thermal core plus a superthermal population. The physical origin of the superthermal or halo population is still not entirely understood to this day. In the literature, most theories rely on altitude-dependent collisional dynamics. However, in our recent works (Yoon et al. 2006; Rhee et al. 2006) we put forth an alternative mechanism for the generation of superthermal particles. In this view collective turbulent processes are responsible for acceleration of the electrons to superthermal energies. By solving weak turbulence kinetic equations we have demonstrated that the self-consistent electron VDFs indeed feature κ-like superthermal energetic tails, thus confirming that the turbulent acceleration is a viable explanation for the generation of a superthermal core population.

The motivation for the present discussion stems from the fact that the actual electron VDFs measured in the solar wind (and to some degree, in the upstream region of the bow shock) often feature highly asymmetric forms such that they cannot be simply fit by κ-models. In the present paper, we have thus generalized our theory to include a pair of initially counterstreaming energetic but tenuous electron beam populations. On the basis of such an initial configuration, we have demonstrated that a wide variety of asymmetric energetic tail distribution may result. It is found that the asymmetric tail distribution is reminiscent of the typical electron distribution detected near 1 AU in the solar wind.

When the forward- and backward-propagating components of the tenuous energetic electrons interact with low-energy core solar wind electrons Langmuir turbulence is excited. The ensuing nonlinear wave-wave and wave-particle interactions are shown to lead to asymmetric high-energy tail distributions. By numerically solving nonlinear weak turbulence equations for electrons and Langmuir turbulence over a range of physical input parameters, we have identified that the delicate difference in the counterstreaming beam speeds is the main cause for generating the asymmetry in the energetic tail, and that the difference in the counterstreaming beam density ratio is immaterial. The present finding may provide a useful diagnostics for the in situ measurement of the solar wind electrons.

The research at the University of Maryland was supported by NSF grant ATM0535821. This work has been partially supported by the Brazilian agencies Conselho Nacional de Desenvolvimento Científico e Tecnológico (CNPq) and Fundação para o Amparo da Pesquisa no Estado do Rio Grande do Sul (FAPERGS).

REFERENCES

Canullo, M. V., Costa, A., & Fontáin, C. F. 1996, ApJ, 462, 1005
Dorelli, J. C., & Scudder, J. D. 2003, J. Geophys. Res., 108, 1294, DOI: 10.1029/2002JA009484
Ergun, R. E., et al. 1998, ApJ, 503, 435
Feldman, W. C., Asbridge, J. R., Bame, S. J., Montgomery, M. D., & Gary, S. P. 1975, J. Geophys. Res., 80, 4181
Fitzenreiter, R. J., Ogilvie, K. W., Chornay, D. J., & Keller, J. 1998, Geophys. Res. Lett., 25, 249
Fitzenreiter, R. J., Scudder, J. D., & Klimas, A. J. 1990, J. Geophys. Res., 95, 4155
Landi, S., & Pantellini, F. G. E. 2001, A&A, 372, 686
Lie-Svendsen, Ø., Hansteen, V. H., & Leer, F. 1997, J. Geophys. Res., 102, 4701
Lin, R. P., Levedahl, W. K., Lotko, W., Gurnett, D. A., & Scarf, F. L. 1986, ApJ, 308, 954
Lin, R. P., Potter, D. W., Gurnett, D. A., & Scarf, F. L. 1981, ApJ, 251, 364
Mace, R. L., & Hellberg, M. A. 1995, Phys. Plasmas, 2, 2098

Maksimovic, M., et al. 2005, J. Geophys. Res., 110, A09104, DOI: 10.1029/2005JA011119
Montgomery, M. D., Bame, S. J., & Hundhausen, A. J. 1968, J. Geophys. Res., 73, 4999
Nieves-Chinchilla, T., & Viñas, A. F. 2008, J. Geophys. Res., in press, DOI: 10.1029/2007JA012703
Ogilvie, K. W., Burlaga, L. F., Chronay, D. J., & Fitzenreiter, R. 1999, J. Geophys. Res., 104, 22389
Ogilvie, K. W., et al. 1995, Space Sci. Rev., 71, 55
Pagel, C., Crooker, N. U., Larson, D. E., Kahler, S. W., & Owens, M. J. 2005, J. Geophys. Res., 110, A01103, DOI: 10.1029/2004JA010767
Pagel, C., Gary, S. P., de Koning, C. A., Skoug, R. M., & Steinberg, J. T. 2007, J. Geophys. Res., 112, A04103, DOI: 10.1029/2006JA011967
Pierrard, V., Maksimovic, M., & Lemaire, J. 1999, J. Geophys. Res., 104, 17021
———. 2001a, Ap&SS, 277, 195
———. 2001b, J. Geophys. Res., 106, 29305
Pilipp, W. G., Miggennieder, H., Montgomery, M. S., Mühläuser, K.-H., Rosenbauer, H., & Schwenn, R. 1987a, J. Geophys. Res., 92, 1075
———. 1987b, J. Geophys. Res., 92, 1093
Rhee, T., Ryu, C.-M., & Yoon, P. H. 2006, J. Geophys. Res., 111, A09107, DOI: 10.1029/2006JA011682
Saito, S., & Gary, S. P. 2007, J. Geophys. Res., 112, A06116, DOI: 10.1029/2006JA012216
Scudder, J. D., & Olbert, S. 1979a, J. Geophys. Res., 84, 2755
———. 1979b, J. Geophys. Res., 84, 6603
Shodhan, S., Crooker, N. U., Kahler, S. W., Fitzenreiter, R. J., Larson, D. E., Lepping, R. P., Siscoe, G. L., & Gosling, J. T. 2000, J. Geophys. Res., 105, 27261
Summers, D., & Thorne, R. M. 1991, Phys. Fluids B, 3, 1835
Vasyliunas, V. M. 1968, J. Geophys. Res., 73, 2839
Vocks, C., & Mann, G. 2003, ApJ, 593, 1134
Vocks, C., Salem, C., Lin, R. P., & Mann, G. 2005, ApJ, 627, 540
Yin, L., Ashour-Abdalla, M., Bosqued, J. M., El-Alaoui, M., & Bougeret, J. L. 1998, J. Geophys. Res., 103, 29595
Yoon, P. H., Rhee, T., & Ryu, C.-M. 2005, Phys. Rev. Lett., 95, 215003
———. 2006, J. Geophys. Res., 111, A09106, DOI: 10.1029/2006JA011681